Chapter 5

TIRF-FLIM-FRET Engineering a Technique for High Resolution Detection of nAChR Composition and Stoichiometry

nAChR subtypes are selectively expressed in distinct brain regions and cell types based on their subunit composition [7]. Subtle differences in receptor stoichiometry can influence receptor pharmacology and disease states [1, 4, 13, 48]. For example, α6* receptors are an important neuronal nAChR subtype for nicotine reward, and these receptors can assemble with multiple stoichiometries and composition. α6α4β2, α6α4β3β2, α6β2, and α6β3β2 are all possible α6* subtypes [7, 11, 49]. These subtypes are differentially expressed in brain regions important for dependence, mood, and Parkinson's disease. In the interest of drug design, it would be beneficial to not only be able to identify which subunits are present in an expressed receptor but also to determine the position within the nAChR pentamer each subunit occupies. This information would be invaluable for development of future pharmacological agents selective for each receptor composition and stoichiometry.

Determination of nAChR stoichiometry was attempted using FRET between FP labeled nAChR subunits [6, 21-23, 26]. However, the work presented in chapter 4 strongly suggests that FRET measurements performed using sensitized emission are not a direct measurement of assembled receptor stochiometry. Other fluorescence based methods have been applied to stoichiometric determination. Single molecule photo bleaching experiments successfully differentiated both stoichiometries of the α4β2 receptor through the counting of individual bleaching steps of mEGFP molecules fused to the nAChR subunits [50]. Additionally, donor recovery after photo bleaching (DRAP) measured FRET between

nAChR subunits for determination of receptor composition [21-22]. None of these methods have the sensitivity to determine the position of a donor with respect to an acceptor fluorophore within the pentamer, and interpretation of data is often complicated by background fluorescence from unpaired, unassembled subunits within the cell.

Fluorescence Lifetime Imaging Microscopy (FLIM) offers higher sensitivity FRET measurements over the sensitized emission techniques described in chapter 4. Sensitized emission relies on detection of both donor and acceptor intensity for calculation of E_{FRET}. FRET detection by FLIM is dependent only on changes in the lifetime of the donor fluorophore and is therefore a more direct measurement. By definition, FRET is an alternative path of fluorescent decay for an excited donor molecule to an acceptor molecule in the ground state. This non-radiative transfer of energy reduces the occupancy time (or lifetime) of the donor molecule in the excited state and this shorting of fluorescence lifetime can be measured and quantified. The efficiently of FRET (E_{FRET}) can be calculated for donor and acceptor molecules of single exponential decay and fixed distance using equation 10, where τ_D is the fluorescent lifetime of the donor fluorophore, and τ_{DA} is the lifetime of the donor in the presence of a FRET acceptor [40, 51].

(eq. 10) $$E_{FRET} = 1 - \frac{\tau_{DA}}{\tau_D}$$

The singular dependence on donor lifetime for FRET measurement via FLIM not only eliminates the problem of background and bleed-through fluorescence from unpaired subunits, but generation of a time-correlated single-photon-counting (TCSPC) histogram yields additional information about the percentage of donor fluorophores experiencing

FRET [52-53]. TCSPC is the most common detection method for FLIM, and it allows calculation of fluorescent lifetimes by measuring the time difference between a single laser pulse and the detection of an emitted photon by a photo-multiplier tube (PMT) or other detection device. These detection events are then binned and plotted across time points and the resulting histogram is the fit to one or more exponential decay curves from which fluorescence lifetimes (τ) can be extracted [52].

Preliminary experiments measuring FRET by FLIM using TCSPC and confocal microscopy led to challenges to data interpretation that were similar to those seen with other methods using confocal microscopy: FRET signals were homogenous for all experimental conditions and it was impossible to determine differences in receptor composition (Richards and Sedak 2011, unpublished data). Use of FLIM eliminates the problem of bleed-through fluorescence from directly excited acceptor molecules, but it is unable to distinguish fully assembled pentamers from sub-assemblies of nAChR subunits such as dimers, trimers, and tetramers in intracellular compartments visible in a confocal image. We hypothesized that the homogeneity in FRET calculations could be due to these partially assembled subunit complexes that could comprise the majority of the τ_{DA} component.

Only assembled, pentameric receptors are trafficked to the surface of the cell; therefore, Total Internal Reflection Fluorescence (TIRF) microscopy can be used to isolate assembled receptors for visualization. TIRF microscopy exploits the evanescent wave that occurs when the incident beam of light is totally internally reflected at a glass-water interface [54]. The wave penetrates into the cell with an intensity that decays exponentially such that only fluorophores within ≤ 200 nm of the cell surface are excited. TIRF has been

used to selectively excite populations of fully assembled, pentameric nAChRs at the plasma membrane for studies on trafficking and upregulation [23]. TIRF and FLIM have not previously been performed in concert. By combining these techniques (TIRF-FLIM) we have engineered the capability to selectively measure FRET interactions within nAChR pentamers at or near the cell surface for high resolution detection of composition and stochiometry.

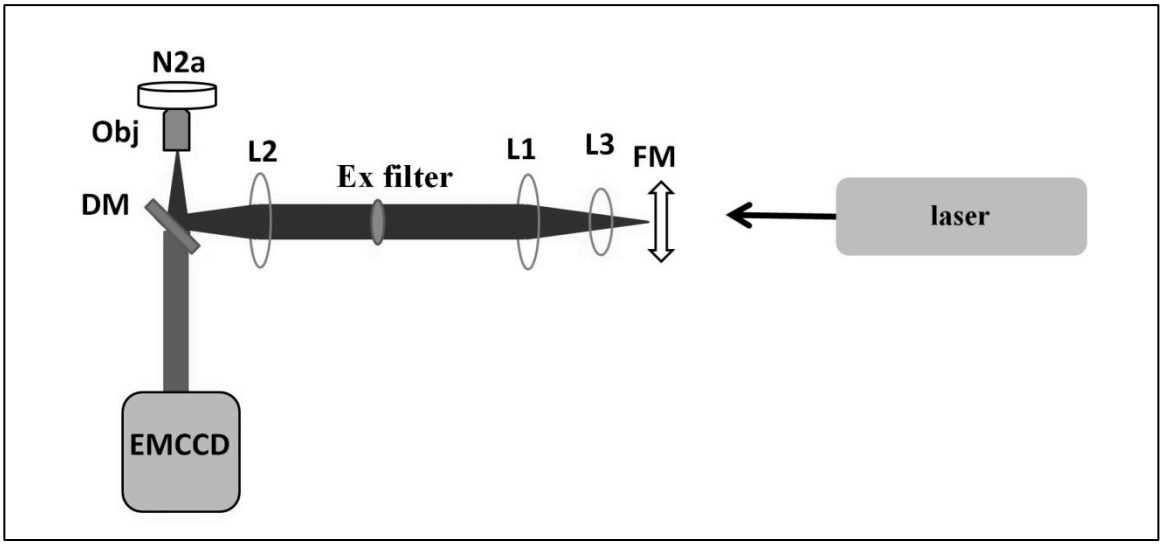

Figure 5.1A
Schematic of a conventional TIRF microscope.
FM = focal mirror, L = lens, Ex filter = Excitation filter, Obj = 100X 1.45 NA oil-immersion objective lens, N2a indicate the sample dish containing N2a cells, DM = dichroic mirror, EMCCD = Olympus CCD camera.

Adaptation of an existing TIRF microscope for TCSPC FLIM detection required several modifications. Figure 5.1A illustrates an Olympus IX81 inverted microscope with TIRF capability [50]. A 488nm picosecond pulsed diode laser (PDL 800-D, PicoQuant GmbH) was mounted to the back port of the microscope and a diverter was added to the outport to re-direct light from the ccd camera to a single photon counting board (PMT) (SPCM-AQR SPAD, Perkin Elmer). The PMT detector was connected to a TCSPC module and event timer (PicoHarp 300, PicoQuant GmbH) and a separate windows PC loaded with PicoHarp 2.0 software (Figure 5.1B).

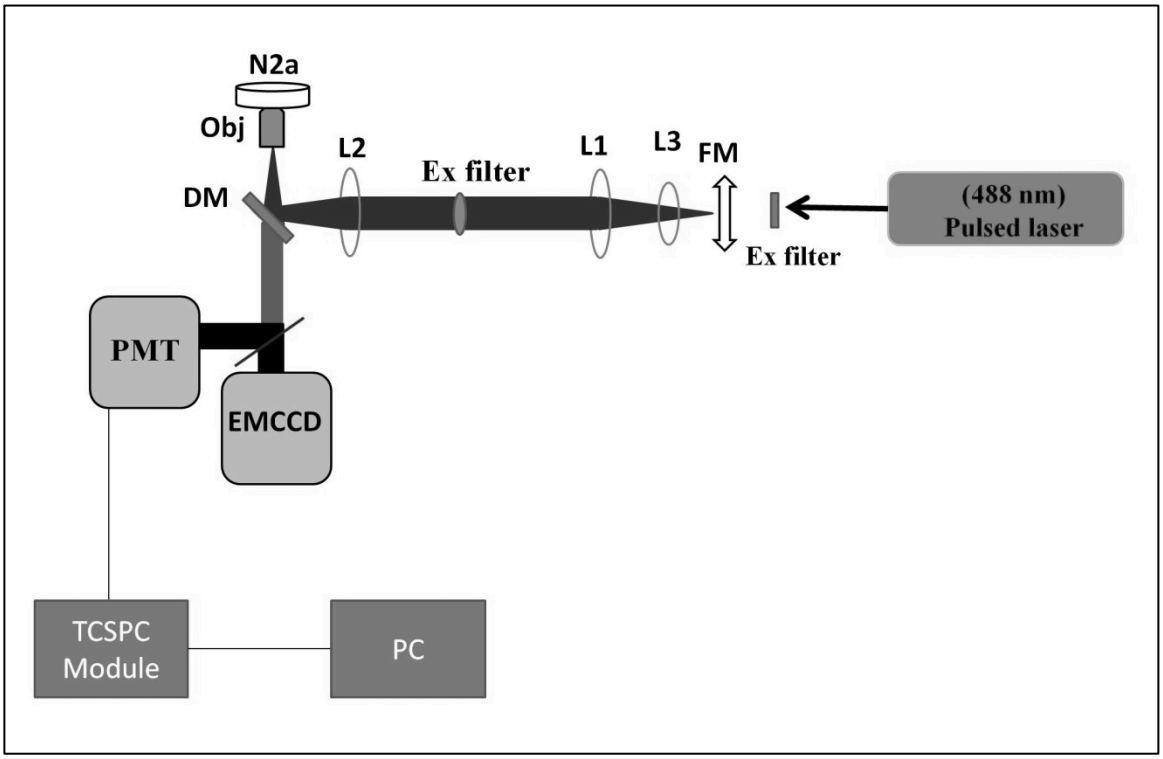

Figure 5.1B
Schematic of modifications made to conventional TIRF microscope for addition of FLIM capability.
FM = focal mirror, L = lens, Ex filter = Excitation filter, Obj = 100X, 1.45 NA oil-immersion objective lens, N2a indicate the sample dish containing N2a cells, DM = dichroic mirror, EMCCD = Olympus CCD camera, PMT = photo multiplier tube. TCSPC Module = time correlated single photon counting module with single event timer, PC = personal windows computer with PicoHarp 2.0 software.

The mouse muscle nAChR was selected as the model receptor for technique validation because, unlike the neuronal nAChRs, it has a fixed stoichiometric composition of $(\alpha 1)_2\beta 1\gamma\delta$ [2, 55]. The fixed nature of the muscle nAChR stochiometry and composition allows measurement of FRET between each geometric relationship within the pentamer. By varying which subunits are fluorescently labeled in expressed receptors, we are able to straightforwardly measure the E_{FRET} values for single-adjacent and single non-adjacent FRET pairs, as well as each multiple donor and acceptor permutation (see figure 5.2). Fluorescent labels were introduced into mouse muscle subunits following methods well described by Lester et al. [6, 21-23].

Table 3 lists the constructed fluorescent subunits. Preliminary FLIM experiments performed using confocal microscopy revealed an inexplicable second lifetime in mEGFP control measurements (Richards and Sadek 2011, unpublished data). However, mYFP consistently displayed a single ~ 2.9 ns lifetime. mYFP was therefore selected as the donor flurophore for TIRF-FLIM experiments with mCherry as the acceptor.

Table 3

Subunit	Fluorescent Protein	Subunit	Fluorescent Protein
α	none	α	mGFP
α	mYFP	α	mYFP Y66C
α	mCherry	α	mYFP Y145W
β	none	β	mGFP
β	mYFP	β	mYFP Y66C
β	mCherry	β	mYFP Y145W
γ	none	δ	mGFP
γ	mYFP	δ	mYFP Y66C
γ	mCherry	δ	mYFP Y145W
δ	none	γ	mGFP
δ	mYFP	γ	mYFP Y66C
δ	mCherry	γ	mYFP Y145W

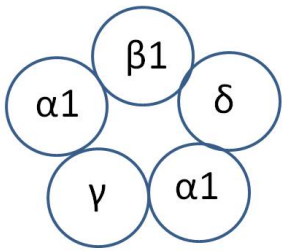

	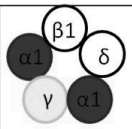	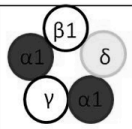	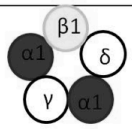	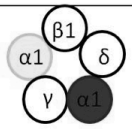	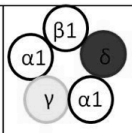	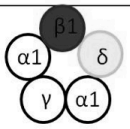	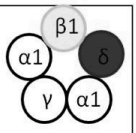
E_{FRET} theoretical	77%	36%	36%	9%	9%	63%	63%
E_{FRET} measured	71.49 ± .55%	71.93 ± .43%	70.26 ± .60%	75.47 ± .64%	73.15 ± .44%	70.24 ± 1.1%	72.47± .47%
FRET Fraction	36.07 ± 1.1%	28.70 ± 1.0%	28.91 ± 2.6%	16.53 ± 1.5%	18.32 ± 1.2%	21.46 ± 1.2%	21.76 ± 2.1%

Figure 5.2
Illustration of some fluorescent muscle receptor stoichiometries and their measured E_{FRET} values. Dark grey fill indicate FRET acceptor (mCherry) and light grey fill indicates FRET donor 9mYFP). No fill indicates no FP tag is present on the subunit. FRET fraction refers to the percentage of donor fluorophores that had shortened lifetimes due to FRET.

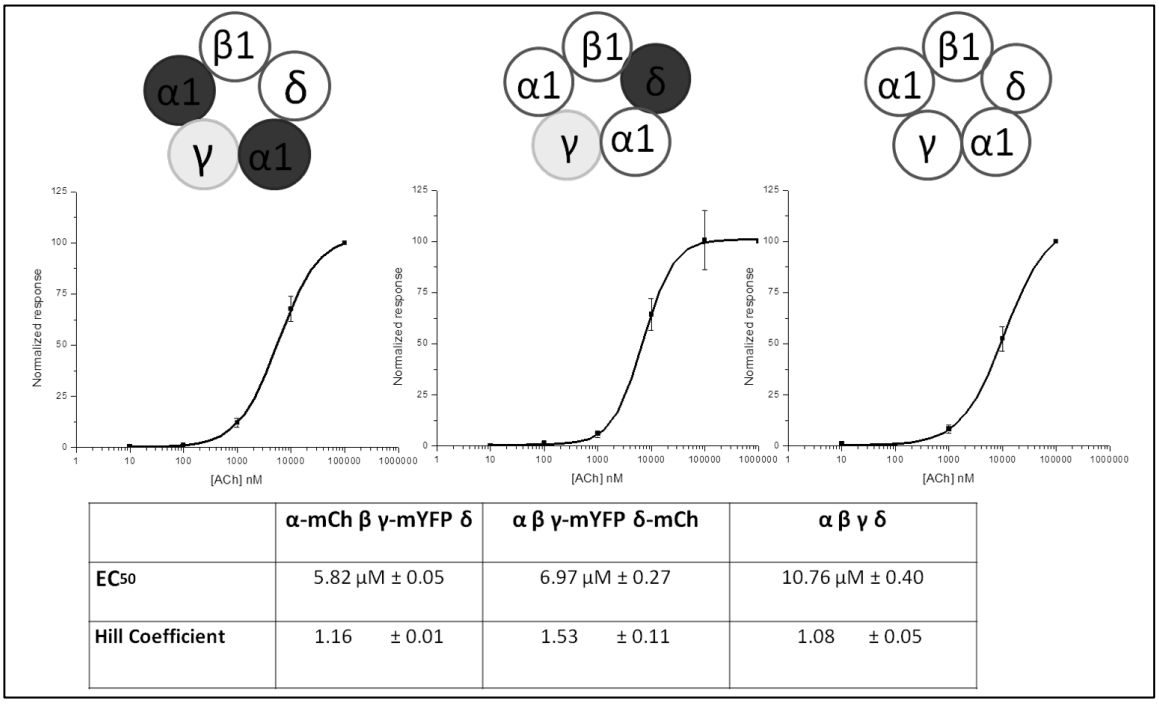

	α-mCh β γ-mYFP δ	α β γ-mYFP δ-mCh	α β γ δ
EC_{50}	5.82 μM ± 0.05	6.97 μM ± 0.27	10.76 μM ± 0.40
Hill Coefficient	1.16 ± 0.01	1.53 ± 0.11	1.08 ± 0.05

Figure 5.3
Acetylcholine dose response curves for muscle nAChRs expressed in differentinated N2a cells 48 h post transfection. Cartoon of receptor pentamer indicates receptor type. Dark grey fill indicates FRET acceptor (mCherry), light grey fill indicates FRET donor (mYFP), no fill indicates no FP label was present on the subunit.

Fluorescent subunits were verified for function using the same methods described in chapter 1. Electrophysiological recordings were performed by Tim Indersmitten on differentiated N2a cells transiently transfected with FP- or non FP-tagged muscle nAChR

subunits. Figure 5.3 displays some of the recorded dose response curves and EC_{50} values for these receptors. Measured EC_{50} were two-fold higher than values reported from *Xenopus* oocytes but these variations could be attributed to the differences in receptor expression system [56]. When fluorescent nAChR subunits were transfected without all the necessary subunits, no measureable currents were seen.

N2a cells were transiently transfected in growth media under serum-starved conditions to encourage differentiation (appendix ii) [57]. Differentiated N2a cells have extended processes and increased adhesion to the glass coverslip. This increased surface area contributes to an improved TIRF signal over non-differentiated N2a cells. Cells were imaged 24 h after transfection in CO_2 buffering Leibovitz media without phenol-Red. Temperature was maintained at 37 ºC during imaging using an incubator installed on the microscope stage and a heating coil that warmed the objective itself to 37 ºC. Samples were excited with 488 nm pulsed laser illumination, and data was collected using a PMT with TCSPC module.

Single cells were imaged at a time. One disadvantage of lifetime imaging with our adapted TIRF microscope is the loss of spacial resolution achieved with scanning confocal. All photons from the exited sample are collected by the PMT as if from a single pixel. An adjustable aperture was used to restrict illumination of the sample to only the cell of interest to avoid contaminant photons from other cells in the field of view. Laser intensity was adjusted to achieve a photon detection rate of approximately 1000 kCounts/s. Sample data was collected for a minimum of 2×10^3 total photons/cell to insure sufficient points for reliable exponential fits of the TCSPC histogram. PicoQuant GmbH proprietary SymPhoTime software was used for all data records and analysis.

Control experiments performed with single mYFP/mCherry FRET pairs revealed inconsistencies in measured mYFP lifetime. In the absence of mCherry the measured lifetime (τ_D) of mYFP maintained an average of 2.9 ns, a number consistent with literature report [58]. However, when mCherry was also present the measured τ_D was artificially shortened and exhibited unusual variability (see figure 5.4). This inconsistency complicated determination of τ_{DA} and perhaps unsurprisingly, E_{FRET} calculated from these fits did not track with theoretical values (see figure 5.2).

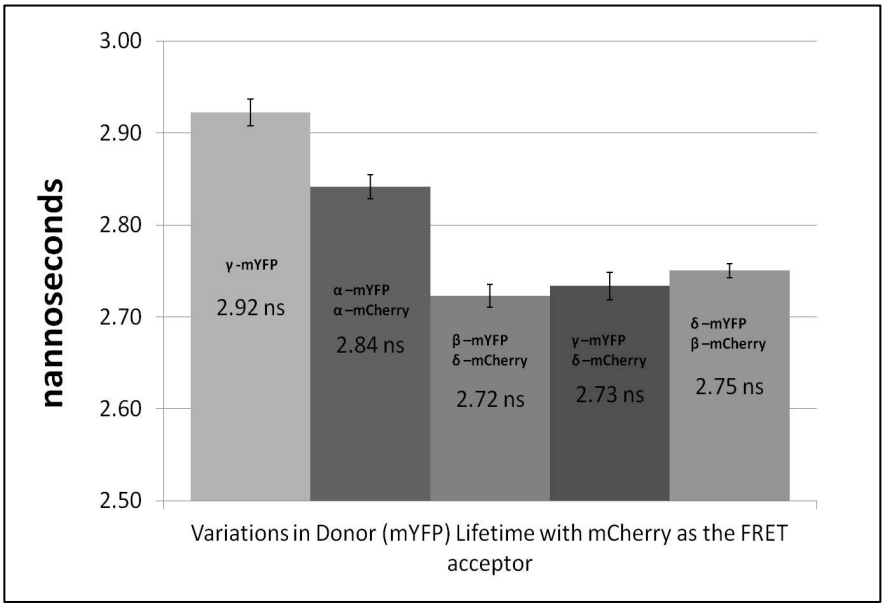

Figure 5.4
Bar graph describing variation in calculated non-FRET lifetimes of mYFP donors in the presence of different mCherry acceptors. It is expected that calculated non-FRET donor lifetime should not change regardless of the presence of a FRET acceptor. This unexpected variability complicated lifetime fits and E_{FRET} calculations.

Significant variability in mYFP lifetime in the presence of mCherry led to investigation into the fluorescent properties of mCherry. It was discovered that mCherry exists in two possible brightness states that correspond to two distinct fluorescence lifetimes [59]. When mCherry is used as a FRET acceptor the energy transfer rate from the donor is different for each brightness state, and equation 10 cannot be applied for calculation of E_{FRET}. We

concluded that mCherry is not an ideal FRET acceptor for FLIM experiments, and a new FRET pair was selected.

mEGFP is the ideal FRET donor for our system. The pulse laser excites at 488nm, a wavelength closer to the absorption maxima of mEGFP (485 nm) than to mYFP (514 nm). Due to lack of success achieving a single exponential fit for a pure population of mEGFP when measured via cofocal microscope, mEGFP was initially disregarded as a potential FRET donor. Indeed, TIRF-FLIM measurements of mEGFP lifetime also yielded a two exponential decay behavior. Acting on a hunch, we hypothesized that the fast, second component contaminant in the mEGFP decay curve could be photons from the laser itself. Addition of a direct excitation filter (474/21) just after the laser in-port and a more stringent emission filter (520/34) eliminated the second lifetime component. With these modifications, a single component decay curve (τ = 2.8 ns) was achieved for a pure population of mEGFP labeled nAChR subunits.

This advance allowed us to proceed using the mYFP as the FRET acceptor. The large blue-shifted tail of the mYFP absorbance spectra does not make mYFP an ideal acceptor for traditional FRET applications because of direct excitation of mYFP by the 488 nm laser. Direct excitation depopulates the fluorescent acceptor molecules in the ground state that can be excited through FRET by mEGFP. This fluorescence bleed through contaminates detection of FRET by sensitized emission (equation 8 chapter 4). FLIM only measures behavior of the donor fluorophore and therefore we are not concerned with the emission of acceptor fluorescence. mYFP can therefore be used as a FRET acceptor for FLIM.

Besides the assumption of single lifetime decays, equation 10 requires that the donor and acceptor fluorophores be separated by a fixed distance. The FP labels reside in the long flexible M3-M4 loop region of the nAChR subunits. It is possible that the flexibility of these unstructured regions allows enough movement of the fluorophores that this condition is not satisfied. Introduction of steric constraints in the intracellular loop regions may restrict movement of the FP labels and improve E_{FRET} calculations. A dark XFP variant would be useful for this purpose because such a label would retain identical properties to the mEGFP and mYFP proteins without addition of another fluorescent species to the experimental system.

mYFP-Y66C is a mutant variant of YFP that is unable to form a functional chromaphore due to cysteine substitution at a crucial Y66 residue. Therefore, mYFP-Y66C has the same properties of mYFP but is unable to absorb or emit fluorescence [60]. Using mYFP-Y66C as a "place-holder" label on subunits that are not labeled with a FRET donor or FRET acceptor allows us to apply the distance assumptions proposed by Son et al. [6]. We hypothesize that expression of mouse muscle nAChRs containing mEGFP, mYFP, or mYFP-Y66C labels on subunits in fixed relationships within the pentamer will satisfy the system requirements as dictated by equation 10.

N2a cells were transfected with mouse muscle nAChR subunits, each bearing a mEGFP, mYFP, or mYFP-Y66C fluorescent label. Visualization with TIRF microscopy 24h post-transfection revealed little or no receptor expression on the plasma membrane. Pseudo-TIRF images of differentiated N2a cells expressing muscle nAChR pentamers illustrate the challenges to expressing a fully labeled receptor. It appears that when all five

subunits contain a FP label, receptor expression on the plasma membrane is severely impaired (figure 5.5).

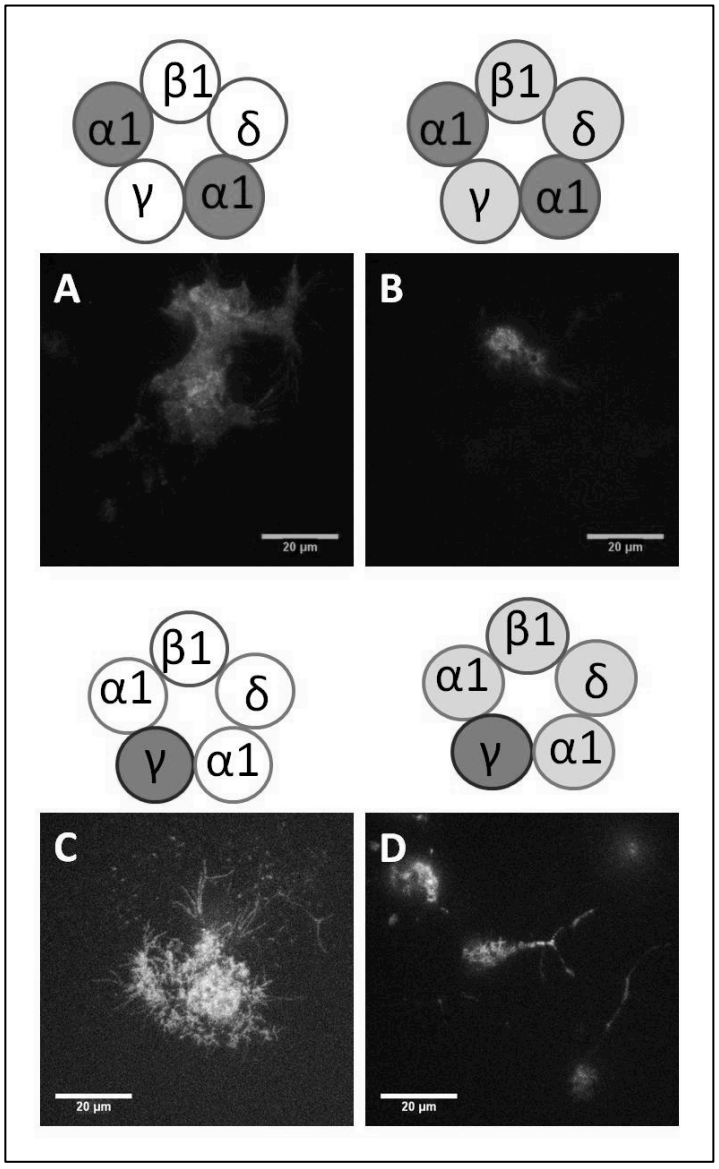

Figure 5.5
Example TIRF images of differentiated N2a cells expressing fluorescent nAChRs. Images were taken 48 h post transfection after excitation at 488 nm. Dark grey fill indicates fluorescent subunits. Light grey fill indicates subunits with mYFP-Y66C labels.
A. α1-mEGFPβ1γδ shows strong expression and clear membrane fluorescence
B. α1-mEGFP(β1γδ) -mYPF-Y66C shows only intracellular expression and little to no membrane fluorescence.
C. α1β1γ-mYFPδ shows strong surface expression and clear membrane fluorescence.
D. γ-mYFP(α1β1δ)-mYFP-Y66C shows only intracellular expression and little to no membrane fluorescence.
These data indicate that fully labeled muscle nAChRs do not traffic to the plasma membrane.

Fully labeled neuronal nAChRs such as α4-mEGFPβ2-mCherry have successfully been expressed in N2a cells and imaged using TIRF [23, 50]. It is unclear why expression of the labeled muscle nAChR was unsuccessful. A possible hypothesis is that the FP labels obscured protein sequences in the M3-M4 loop that are important for receptor trafficking.

Trafficking motifs in the neuronal beta subunits are important for membrane expression [23]. We examined sequences of muscle β1, and the neuronal β2 and β4 M3-M4 loops to determine if FP interference with trafficking signals could be the cause of aberrant expression of fully labeled muscle nAChR (figure 5.6). Figure 5.6 displays the alignment of M3-M4 loop sequences for β1, β2, and β4. No trafficking motifs were identified in the β1 sequence. It is possible that the muscle receptors contain as yet unidentified motifs important for vesicular transport of assembled receptors to the plasma membrane.

```
          mouse β2 KVVFLEKLPTLLFLQQPRHRCARQRLRLRRRQREREGAGTLFFREGPAAD
          mouse β4 KECFLHKLPTFLFMKRPGLEVSPARVPHSSQLHLTTAEATSTSALGPSSP
mouse muscle β1 RQIFIHKLPPYLGLKRPKPERDQLPEPHHS-LSPRSGWGRGTDEYFIRKP
```

Figure 5.6
Alignment of mouse beta M3-M4 loops. Mouse β2 contains both a forward trafficking LFM and an ER retention RRQR sequence (bold), and mouse β4 contains only an IFM sequence (bold). No trafficking sequences were identified in the mouse muscle β1 M3-M4 loop.

It is obvious that optimization of labeled muscle nAChR expression must occur before FLIM-FRET experiments are attempted. Approaches to improving surface expression of the labeled receptors include movement of the FP insertion location within the M3-M4 loop, extension of the flanking linker sequence to allow space for interaction with protein components of the vesicular transport system, and expression in a non-neuronal cell type. Complete analysis of M3-M4 loop sequences of the muscle nAChR subunits was performed before insertion of FP labels and care was taken to avoid any motifs know to be important for processing and transport of the receptor. It is possible that these subunits contain as yet unidentified sequences that perform this signaling function. If so, construction of additional fluorescent muscle subunits with FP inserted into alternative M3-M4 loop may avoid disruption of these unidentified sequences and restore proper trafficking and function to the labeled receptor.

It may also be the case that the FP insertion does not disrupt an unknown trafficking signal but that the presence of a FP label on all five subunits obscures access of trafficking proteins to these signal sequences. If this is the case, significant extension of the G-A-G and A-G-A linkers flanking the inserted FP gene may enable proper identification of trafficking motifs and successful membrane expression. Lastly, it is possible that heterologous expression of muscle type nAChRs is more efficient in muscle derived cell lines. Differentiated N2a cells were selected for use in these experiments due to the large surface area of the cell in contact with the imaging cover slip. This is ideal for TIRF imaging but may not be optimal for muscle receptor expression. A cell type derived from a muscle lineage may be more successful at expression of muscle nAChRs. c2c12 cells are derived from mouse muscle myoblasts and can express fluorescently labeled nAChRs. These cells may be a more amenable expression system for fully labeled muscle nAChRs.

In this chapter, we have described unique fluorescent protein constructs for the study of mouse muscle nAChRs and necessary modifications for detection of FRET using TIRF-FLIM imaging. We have also generated the first data from the application of TIRF-FLIM imaging to FRET detection within nAChRs. If the described challenges to this new technique are met, TIRF-FLIM-FRET may be a promising method for differentiation of nAChR receptor stoichiometry. It remains to be seen if the constraints of the biological system allow determination of donor position within the receptor pentamer using this technique.